RESEARCH ARTICLE

WILEY

Investigating functional changes in the brain to intermittently induced auditory illusions and its relevance to chronic tinnitus

Anusha Mohan[1] [ID] | Neil Bhamoo[2] | Juan S. Riquelme[2] | Samantha Long[2] | Arnaud Norena[3] | Sven Vanneste[1,2]

[1]Global Brain Health Institute & Institute of Neuroscience, Trinity College Dublin, Dublin, Ireland

[2]Lab for Clinical & Integrative Neuroscience, School of Behavioral and Brain Sciences, The University of Texas at Dallas, Dallas, Texas

[3]Laboratory of Sensory and Cognitive Neuroscience, Aix-Marseille University, Marseille, France

Correspondence
Sven Vanneste, Lab for Clinical & Integrative Neuroscience, School of Psychology, Global Brain Health Institute, Institute of Neuroscience, Trinity College Dublin, College Green 2, Dublin, Ireland.
Email: sven.vanneste@tcd.ie

Funding information
University of Texas at Dallas Dean's Award

Abstract

Several studies have demonstrated the neural correlates of chronic tinnitus. However, we still do not understand what happens in the acute phase. Past studies have established Zwicker tone (ZT) illusions as a good human model for acute tinnitus. ZT illusions are perceived following the presentation of a notched noise stimulus, that is, broadband noise with a narrow band-stop filter (notch). In the current study, we compared the neural correlates of the reliable perception of a ZT illusion to that which is not. We observed changes in evoked and total theta power in wide-spread regions of the brain particularly in the temporal-parietal junction, pregenual anterior cingulate cortex/ventromedial prefrontal cortex (pgACC/vmPFC), parahippocampus during perception of the ZT illusion. Furthermore, we observe that increased theta power significantly predicts a gradual positive change in the intensity of the ZT illusion. Such changes may suggest a malfunction of the sensory gating system that enables habituation to redundant stimuli and suppresses hyperactivity. It could also suggest a successful retrieval of the memory of the missing frequencies, resulting in their conscious perception indicating the role of higher-order processing in the mechanism of action of ZT illusions. To establish a more concrete relationship between ZT illusion and chronic tinnitus, future longitudinal studies following up a much larger sample of participants who reliably perceive a ZT illusion to see if they develop tinnitus at a later stage is essential. This could inform us if the ZT illusion may be a precursor to chronic tinnitus.

KEYWORDS
ERP, sLORETA, time–frequency decomposition, Zwicker tone

1 | INTRODUCTION

Perception is a top-down process for interpreting the nature and meaning of bottom-up sensory stimuli (Schacter, 2011). In the event of decreased bottom-up input, the brain finds alternate mechanisms to compensate for the change in incoming information relying more on top-down factors such as memory and cues from other sensory modalities, thus modifying perception (Friston, 2010; Mohan & Vanneste, 2017). This compensation for decreased input can manifest as the perception of the expected but missing stimulus in that specific sensory domain, called phantom perception (Mohan & Vanneste, 2017). Tinnitus is the simplest kind of auditory phantom perception,

where people report a ringing or buzzing in their ear (Jastreboff, 1990). Tinnitus can be a debilitating disorder commonly accompanied by noise-related or age-related hearing loss (König, Schaette, Kempter, & Gross, 2006; Negri & Schorn, 1991; Peelle & Wingfield, 2016) affecting several million people all over the world. Chronic tinnitus is widely studied in humans using neuroimaging, electrophysiological, and both invasive and noninvasive neuromodulation techniques (Claes, Stamberger, Van de Heyning, De Ridder, & Vanneste, 2014; De Ridder, Congedo, & Vanneste, 2015; De Ridder & Vanneste, 2014; Hullfish, Abenes, Yoo, De Ridder, & Vanneste, 2019; Hullfish et al., 2018a, 2018b; Husain et al., 2011; Mohan, Alexandra, Johnson, De Ridder, & Vanneste, 2018; Mohan, De Ridder, Idiculla, DSouza, & Vanneste, 2018; Mohan, De Ridder, & Vanneste, 2016, 2017). However, the acute phase of tinnitus has received relatively little attention. Inducing tinnitus in humans has its ethical issues and hence researchers have relied instead on animal models (Dehmel, Eisinger, & Shore, 2012; Jastreboff, Sasaki, & Brennan, 1988; Noreña, 2011; Wang, Brozoski, & Caspary, 2011). Animals are subjected to a blast of loud noise that produces noise-induced hearing loss. The presence of tinnitus is screened by the ability of the animal to detect gaps embedded into a continuous stream of noise (Turner et al., 2006). The hypothesis is that animals with tinnitus have worse gap detection thresholds compared to controls. This is attributed to them perceiving a ringing in the ear during those gaps. However, since tinnitus is both subjective and heterogeneous (Cederroth et al., 2019), there is an ongoing debate as to whether neural correlates of tinnitus in animals correspond to the tinnitus percept or to the hearing loss.

One potential solution to this debate is the Zwicker tone (ZT) illusion, which has been shown to serve as a good proxy for acute tinnitus in humans because of several similarities in their acoustic and neurophysiological correlates (Norena, Micheyl, & Chery-Croze, 2000). The ZT illusion is an auditory afterimage perceived following the presentation of a notched-noise stimulus (Norena & Eggermont, 2003; Zwicker, 1964). Previous studies have shown that, like tinnitus, the ZT illusion is accompanied by an increased nonlinear gain in the central nervous system created by the silent frequencies of the notched-noise stimulus (Parra & Pearlmutter, 2007; Zeng, 2013). This was shown to be a result of remodeling lateral inhibition in the auditory pathways, with neurons responding to the frequencies surrounding the notch (Catz & Noreña, 2013; Norena et al., 2000; Norena & Eggermont, 2003), a finding consistently shown in animal models of tinnitus (Shore, Roberts, & Langguth, 2016). This claim was further supported by studies showing a decrease in alpha activity and an increase in beta/gamma activity in the auditory cortex in response to notched-noise stimuli that elicited a ZT illusion (Leske et al., 2014). The hyperactivity of the auditory cortex also correlated with the loudness of the illusion (Leske et al., 2014). Such patterns of activity are neural signatures of aberrant thalamocortical rhythms, illustrating reduced inhibition of unwanted stimuli in tinnitus patients (De Ridder, Vanneste, Langguth, & Llinas, 2015; Llinás, Ribary, Jeanmonod, Kronberg, & Mitra, 1999; Llinás, Urbano, Leznik, Ramírez, & van Marle, 2005). Inhibition of unwanted and irrelevant stimuli is controlled by a frontostriatal and medial temporal sensory gating system

(Krause, Hoffmann, & Hajós, 2003; Rauschecker, Leaver, & Muhlau, 2010; Rauschecker, May, Maudoux, & Ploner, 2015).

In addition to receiving bottom-up projections from the auditory pathways, the auditory cortex also receives top-down frontostriatal projections from the nucleus accumbens (NAc) via the pregenual anterior cingulate cortex/ventromedial prefrontal cortex (pgACC/vmPFC) and dorsolateral prefrontal cortex (DLPFC; Rauschecker, Leaver, & Mühlau, 2010). These regions are proposed to exercise top-down inhibition to decrease the hyperactivity in the auditory cortex (Rauschecker et al., 2015; Rauschecker, Leaver, & Mühlau, 2010). This process happens at the level of the thalamus and thus a fully functional "noise-cancelation" system would not permit unwanted stimuli to be relayed to the auditory cortex (Rauschecker, Leaver, & Mühlau, 2010). Consistent with this idea, tinnitus patients with and without hearing loss exhibit an increase in theta activity in the pgACC/vmPFC region, showcasing a disinhibition of unwanted stimuli and a failed noise-cancelation system (Vanneste, Alsalman, & De Ridder, 2018; Vanneste, Alsaman, & De Ridder, 2018).

Furthermore, gating of unwanted information by the regions of the medial temporal lobe is performed by their direct corticocortical connections with the auditory cortex. Decreased sensory gating is associated with disinhibition of repetitive stimuli and is accompanied by increased theta activity in the hippocampus (Krause et al., 2003). A consistent finding is reported in tinnitus and schizophrenic patients (Campbell, Bean, & LaBrec, 2018; Freedman et al., 1996; Hong, Summerfelt, Mitchell, O'Donnell, & Thaker, 2012). During resting state, tinnitus patients with hearing loss show increased theta activity in the medial temporal regions such as the hippocampus and parahippocampus, suggesting a malfunctioning of the sensory gating system and a dishabituation to irrelevant and redundant auditory stimuli (De Ridder et al., 2014; De Ridder & Vanneste, 2014; De Ridder, Vanneste, & Freeman, 2014). The parahippocampus is also a known site for storing auditory memory (Munoz-Lopez, Mohedano-Moriano, & Insausti, 2010).

A complementary theory supporting the hyperactivity in response to the virtual deafferentation (noise notch) and the generation of the ZT illusion is the Bayesian brain model (De Ridder, Vanneste, & Freeman, 2014; Hullfish, Sedley, & Vanneste, 2019; Sedley, Friston, Gander, Kumar, & Griffiths, 2016; Vilares & Kording, 2011). The idea, in brief, is that the brain is exposed to various stimuli that it uses to create a predictive internal model of the environment (Friston, 2005). Discrepancies between the model and incoming stimuli generate prediction error signals (Friston et al., 2016; Friston, Kilner, & Harrison, 2006). These prediction errors create an uncertainty in the brain which is minimized by appropriately managing it (Knill & Pouget, 2004; Vilares & Kording, 2011). The prediction error is either suppressed, compensated or the model is updated to predict the new stimulus (De Ridder, Vanneste, & Freeman, 2014; Mohan & Vanneste, 2017). The theory of the Bayesian brain may be translated to the perception of the ZT illusion by considering that the ZT stimulus contains a band of attenuated frequencies sending a relative decrease of input to the brain. The relative reduction in information creates a prediction error that is suppressed by the auditory illusion of the missing

frequencies. Per this theory, the hyperactivity in auditory regions reflects increased prediction errors in the brain (Hullfish, Sedley, & Vanneste, 2019; Sedley et al., 2015; Sedley, Friston, et al., 2016). Additionally, increased theta activity in the parahippocampus is proposed to reflect pulling out the missing frequencies from memory as a compensation to minimize the increased prediction error (De Ridder, Elgoyhen, Romo, & Langguth, 2011; De Ridder, Vanneste, & Freeman, 2014; Munoz-Lopez et al., 2010).

Most of the above are however studies examining the resting-state activity in tinnitus patients. Although resting-state studies offer insight about the ongoing spontaneous electrical activity in the brain, they cannot tease apart specific neural constructs. Inducing an auditory illusion in a group of healthy young adults gives us a controlled environment to examine changes in the brain during the perception of an auditory phantom. The changes in neural activity particular to a specific event are measured using event-related potentials (ERPs; Cohen, 2014; Winkler, Denham, & Escera, 2013). ERPs measure the causal changes in neural activity relative to the onset of the event and are characterized by specific components (Cohen, 2014). In the current study, we aim to understand if changes in the sensory gating system are characteristic only of chronic tinnitus, or if they may be an underlying mechanism accompanying perception of acute auditory illusions that may serve as a proxy for acute tinnitus. To do this, we compare the ERPs to personally tailored ZT illusion eliciting stimulus, a white noise stimulus (no notch), and an active control stimulus (white noise with a notch which does not elicit a ZT illusion) in a group of healthy young adults who can and cannot reliably perceive the ZT illusion. Furthermore, we perform time-frequency analyses to compare the evoked (ERP-related) and total (combination of ERP and ongoing) theta power between the two groups. Based on the resting-state studies in tinnitus patients which characterize the activity in the brain during the perception of an auditory phantom, we hypothesize that participants reliably perceiving a ZT illusion would also exhibit

increased evoked and total theta activity in the pgACC/vmPFC and medial temporal regions during the perception of the ZT illusion, suggesting a dysregulation of sensory gating system. By understanding the underlying mechanism of action of a potential human model for acute tinnitus, we could speculate that these participants may be at a higher risk of developing chronic tinnitus at a later stage.

2 | MATERIALS AND METHODS

2.1 | Participants

The study involved a group of healthy young adults (N = 47; 17 males, 30 females; M = 20.82 years, SD = 2.60 years) who were screened for tinnitus, Meniere's disease, chronic ear infections, otosclerosis, and several neurological disorders such as tumors, mental disorders, chronic headache, and so forth. Their hearing was tested using pure tone audiometry at 250, 500, 1,000, 2000, 3,000, 4,000, 6,000, and 8,000 Hz, which were obtained according to the procedures prescribed by the British Society of Audiology. Those participants whose hearing threshold at any frequency was greater than 30 dB HL were excluded from the study. Per this criterion, one participant was excluded from the study, leaving us with 46 participants. The participants' mean audiometric thresholds at different frequency bands are visually represented in Figure 1.

2.2 | Stimuli

The stimuli consisted of 3-s-long white noise or notched noise. White noise is defined as a random signal with equal intensity throughout its entire frequency range. The white noise used in the current study was created using frequencies between 0 and 16,000 Hz. A notched noise

FIGURE 1 Demographics and behavioral data. (a) Audiogram showing mean auditory thresholds at different frequencies for all included subjects. The audiogram for the right ear is represented by the red circles and that for the left ear is represented by the blue crosses. (b,c) Comparison of center frequency and width of the noise notch of the ZT eliciting stimulus between the controls (blue) and ZT (red) groups
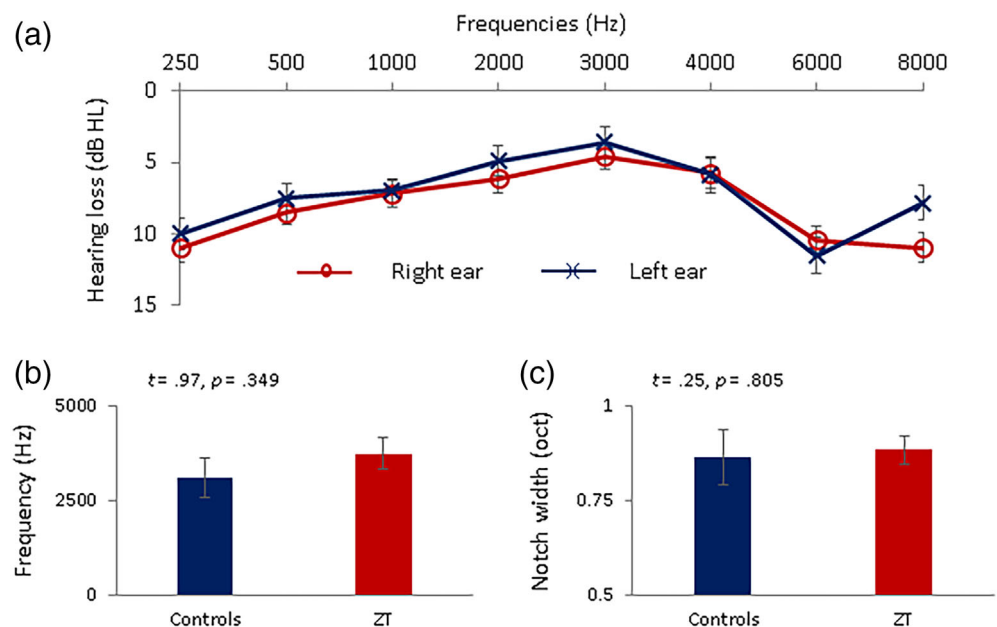
is usually described as white noise with an attenuated band of frequencies surrounding a center frequency. In this study the notched noise stimuli were created using notch bandwidths of 0.4, 0.5, 0.6, 0.75, 0.8, and 1 octave at center frequencies of 1,000, 1,414, 2000, 2,828, 4,000, and 5,657 Hz, respectively. The choice of center frequencies and notch bandwidths is based on a study by Leske et al. (2014). These stimuli were created in MATLAB and were all matched for overall RMS power. The stimuli were played binaurally at 72 dB SPL over stereo headphones.

2.3 | Zwicker tone eligibility pretest

All participants were initially tested for their ability to reliably perceive a ZT illusion. The participants were informed that there would be a sound stimulus followed by a period of silence in which they may or may not be able to hear a ringing in their ears. To determine the participant's ability to perceive a ZT illusion, two types of presentation schemes were used: (Test A) changing the notch center frequency while maintaining constant notch bandwidth; (Test B) changing notch bandwidth while maintaining a constant notch center frequency. The white noise stimuli were interspersed between the notched noise stimuli.

Participants began with Test A, using notched noise stimuli at a fixed 1-octave notch width. This notch width was used here because Leske et al. (2014) found that the intensity rating of the ZT illusion can be modified by changing the notch bandwidth and that the intensity rating was maximal at a 1-octave width. Each trial consisted of a 3-s sound stimulus followed by a 1.5-s silence period. Each center frequency was presented in a series of five trials. A rating screen appeared following the fifth trial when the participant was asked to rate the intensity of the illusion heard in the silence period from 1–7 using a 7-button response pad (1, "no ringing"; 7, "loud and clear"). Each of the center frequencies along with the white noise stimuli were presented twice in a random order. Once the participant rated the loudness of their illusion, a screen with a fixation cross at the center was presented for 2 s followed by the presentation of the five trials of the next stimulus. The center frequency that elicited the highest intensity rating (4 or above) on both repetitions was chosen. If the participant did not rate a ZT illusion 4 or above to the 1-octave noise notch in Test A, then the noise bandwidth was successively reduced and re-tested. If the participant did not perceive a ZT illusion with a rating 4 or above to any of the stimuli until the bandwidth was reduced to 0.5 octaves, then the participant was considered not to produce a reliable ZT illusion.

Participants then went through Test B, where the notch center frequency was kept constant (i.e., at the chosen frequency from Test A) and the notch width was changed to get the precise ZT stimulus for that person. Furthermore, the stimulus that elicited the lowest intensity rating (1 or 2) for each participant was chosen as an active control, that is, a notched noise that did not reliably evoke a ZT illusion.

A reliable ZT illusion was also characterized based on their rating of white noise. Even if people had a 4 or above rating to a notched

noise, if they consistently had a 4 or above rating to white noise as well, then they were not considered to have a reliable ZT illusion. Thus, the participants who were able to consistently and correctly rate the notched and the white noise control stimuli proceeded to the EEG phase of the study (N = 22, M = 20.40 years, SD = 2.70 years, 5 males and 17 females).

2.4 | Main electrophysiological experiment

In the EEG phase of the study, three stimuli were used to evoke different perceptual experiences: (a) the stimulus that produced the most reliable ZT illusion, (b) the notched noise control stimulus to which they produced no ZT illusion (rating 1) or an unreliable ZT illusion (rating 2), and (c) the white noise stimulus. Then, 100 trials of each stimulus were played in a random order. Each trial started with a fixation cross for 3 s. This was followed by each 3 s stimulus and 1.5 s silence period. This was followed by a rate screen where they rated the ringing perceived in the silence period from 1 to 7. The paradigm is visually shown in Figure 2.

2.5 | EEG data collection and preprocessing

Continuous EEG data were collected from each participant in response to the three stimulus conditions played in the ERP paradigm. The data were collected using a 64 channel Neuroscan Synamps[2] Quick Cap configured per the International 10–20 placement system with a reference close to Cz using the Neuroscan Scan 4.5 software. The impedance of each electrode was maintained at <5 kΩ. The data was sampled using the Neuroscan Synamps[2] amplifier at 500 Hz with
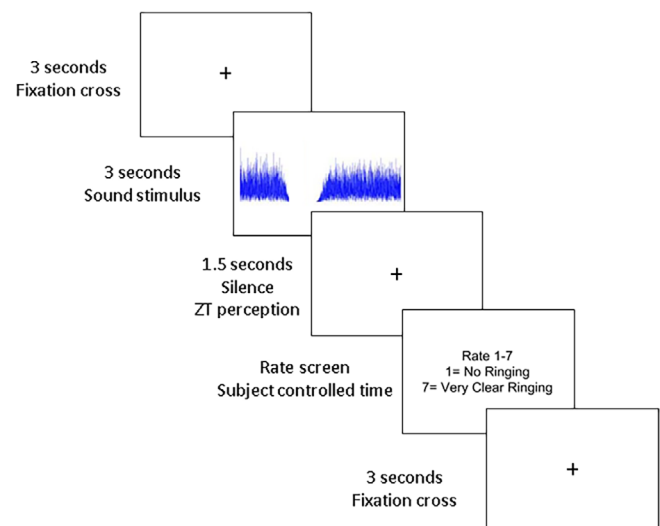

FIGURE 2 Summary of the ERP paradigm. A fixation cross is presented for 3 s followed by the stimulus for 3 s. A 1.5 s silence period is provided to assess the perception of a ZT illusion. The rating of the percept is asked for following the completion of the silence period

online band-pass filtering at 0.1–0.70 Hz. The stimuli were presented through the Neuroscan Stim II system which triggered the Scan 4.5 software every time a stimulus was presented.

Data were then preprocessed using MATLAB and EEGLAB. The preprocessing pipeline included removing of disconnected and unused channels, re-referencing to an average reference, and bandpass filtering using a zero-phase 3,115-point basic Hamming-windowed sinc FIR filter with the lower edge of the frequency pass band at 0.53 Hz and higher edge of the frequency pass band at 55 Hz and a transition bandwidth of 0.53 Hz. The resulting filter passband edges at the −6 dB cut-off was 0.26 Hz and 55.6 Hz. Data from the remaining electrodes after removal of disconnected and unused channels were then subjected to temporal independent component analysis (ICA) using an infomax algorithm (Jung, Makeig, Bell, & Sejnowski, 1998), which was used to remove muscle artifacts, eye blinks, saccades and other noise transients. The mean and standard deviation of the number of removed ICs for the control group is M = 13.28, SD = 1.49 and for the ZT groups is M = 12.55, SD = 3.04. The mean and standard deviation of the number of bad channels removed for the control group is M = 4.43, SD = 2.30 and for the ZT group is M = 4.22, SD = 1.79.

The data were epoched between −1,000 to +6,000 ms relative to the onset of the stimulus. A baseline correction of 200 ms was applied to the data. Artifact detection using a simple voltage threshold of ±90 μV was applied to all epochs and those epochs that did not fall within this threshold were excluded. The mean and standard deviation for the number of trials removed for the ZT stimulus in control group is M = 39.28, SD = 16.71 and the ZT group is M = 27.88, SD = 13.31, for the white noise stimulus for the control group is M = 30.00, SD = 15.83 and for the ZT group is M = 19.00, SD = 11.43 and for the active control notched noise stimulus for the control group is 36.71,

SD = 20.63 and for the ZT group is M = 23.88, SD = 15.67. The final trial numbers for each participant is given in Table 1. Furthermore, an independent t-test is performed to compare the number of ICs, channels, and trials for each condition removed between the two groups. The removed channels were then interpolated using a spherical interpolation algorithm in EEGLAB to ensure all participants had equal number of channels.

2.6 | EEG postprocessing

The consistency of the ratings to the stimuli in the ERP phase was analyzed post hoc. At this stage, participants who rated 4 or above to the ZT stimulus and 3 or below to both the white noise and notched noise controls in at least 50% of the respective trials were sorted into the ZT group. These rating thresholds were based on the average ratings in the study by Leske et al. (2014). Participants who rated 3 or below to the ZT stimulus but also rated 3 or below to the white noise and notched noise control stimuli in at least 50% of the respective trials were sorted into a control group. All other participants were excluded from the remainder of the study since they were considered to have failed to produce a reliable response when the stimuli were presented in a random order. This left us with seven people in the control group (M = 20.71 years, SD = 2.43 years, 1 male and 6 females) and nine people in ZT group (M = 20.33 years, SD = 3.57 years, 2 males and 7 females). The mean center frequency and width of the notch of the ZT eliciting stimulus that was selected from Test A and their audiograms were compared across the two groups using an independent samples t-test and repeated measures ANOVA, respectively.

The entire time sweep of the averaged ERPs of the onset (ERP to the 3-s stimulus presentation) and offset (ERP to the 1.5-s silent

TABLE 1 Final trial numbers for each participant in the ZT, white noise and notched noise stimulus conditions

Group	Subject number	ZT stimulus	White noise stimulus	Notched noise stimulus
Controls	Subject 1	59	69	41
Controls	Subject 2	46	43	35
Controls	Subject 3	70	74	88
Controls	Subject 4	80	87	81
Controls	Subject 5	50	82	80
Controls	Subject 6	81	80	62
Controls	Subject 7	39	55	56
ZT	Subject 1	66	86	80
ZT	Subject 2	69	70	66
ZT	Subject 3	76	74	58
ZT	Subject 4	93	94	94
ZT	Subject 5	79	95	96
ZT	Subject 6	61	76	56
ZT	Subject 7	90	94	90
ZT	Subject 8	58	76	82
ZT	Subject 9	57	65	63

period following stimulus presentation) responses for each stimulus (white noise, notched noise, and ZT-eliciting stimulus) from all channels were compared between the two groups using cluster-based statistics in FieldTrip in accordance to the methods published by Oostenveld and Maris (2007). For every sample (i.e., a channel-time point pair), the two groups are compared by means of a *t*-value that quantifies the effect at the sample. All the samples whose *t*-value have a probability <.05 are selected. The selected samples are clustered in sets based on spatial and temporal adjacency. Cluster-level statistics are calculated by taking the sum of the *t*-values within every cluster. The maximum of the cluster-level statistics is considered and controlled for multiple comparisons by means of Monte–Carlo permutation testing using 5,000 randomizations. A two-tailed *t*-test was used in the cluster statistics and this generated positive and negative clusters for each test. The largest cluster was considered for further correction. A Benjamini–Hoschburg correction with a False Discovery Rate (FDR) level of 0.25 was used to further correct for the 12 comparisons made (2-time frames (onset and offset responses)) × 3 stimuli × 2 clusters (positive and negative clusters)). The mean amplitude of the significant channel-time point pairs from the onset/offset responses of each stimulus condition was compared between the two groups using a repeated-measures ANOVA with group as the between-subject variable and condition (onset/offset response of a stimulus) as the repeated measure.

2.7 | Source reconstruction

The trial averages of the significant onset and offset responses for the different stimuli from each participant was source localized using standardized low-resolution electromagnetic tomography (sLORETA), which estimates the source of the signal (Pascual-Marqui, 2002). sLORETA computes the current density at the source of the signal without assuming a predefined number of sources. A common average reference transformation was applied prior to the application of the source localization algorithm. The solution space for the algorithm used in this study along with the lead field matrix was implemented in the LORETA-Key software (freely available at http://www.uzh.ch/keyinst/loreta.htm). This software implements the standard electrode positions from the MNI-152 scalp (Montreal Neurological Institute, Canada; Jurcak, Tsuzuki, & Dan, 2007) and the lead field produced by Fuchs, Kastner, Wagner, Hawes, and Ebersole (2002) to apply the boundary element method on the T1-weighted MNI-152 template (Mazziotta et al., 2001). Thus, the sLORETA-key anatomical template divides and labels the neocortical (including hippocampus and anterior cingulate cortex) MNI volume into 6,239 voxels each having 5 mm^3 volume based on probabilities returned by the Talairach Daemon Atlas (Lancaster et al., 2000). The co-registration makes use of the correct translation from the MNI-152 space into the Talairach and Tournoux (1988) space (Brett, Johnsrude, & Owen, 2002). The source localized amplitude was averaged across the time points that showed a significant difference in the ERP analysis. This mean amplitude was compared between the two groups through multiple voxel-by-voxel

comparisons using an independent *t*-test. The test was subject to a permutation testing using 5,000 randomizations and was corrected for multiple comparisons using the Bonferroni correction.

2.8 | Time–frequency decomposition

A more in-depth analysis was carried out by performing a time–frequency analysis for the entire time sweep for the onset/offset responses of the stimulus conditions that showed a significant difference between the two groups. A Morlet wavelet convolution (Cohen, 2014) was used to compute the time–frequency decomposition between 2 and 10 Hz on the single-trial EEG data (total power) and the trial averaged ERP data (evoked power) in all the electrodes in order to look at changes in power in the theta frequency defined between 4 and 7.5 Hz. The 2–10 Hz time–frequency decomposition gives room for spectral smearing. A family of Morlet wavelets was created with a linearly increasing number of cycles between 2 cycles at 2 Hz and 4 cycles at 10 Hz sampled at 500 Hz. A baseline normalization (−600 to −300 ms) was employed for both the evoked and total power. For the total power, baseline normalization was done after averaging the power from the single trials. The difference between the total and evoked power is that the evoked power gives the phase-locked component whereas the total power gives the combination of phase-locked and nonphase locked components of time–frequency decomposition (Cohen, 2014). The power was converted to a decibel scale using a log transformation. The choice for baseline normalization was based on Leske et al. (2014). The average total and evoked power of the theta frequency band was calculated as the average theta power over the time points that showed a significant difference in the ERP analysis for each channel in the significant cluster of electrodes. The frequency of interest is consistent with the theta frequency band described in previous resting-state studies in tinnitus (Vanneste, Alsalman, & De Ridder, 2018; Vanneste, Alsaman, & De Ridder, 2018). The total and evoked theta power between 4 and 7.5 Hz averaged over the significant time points in the significant electrode cluster from the ERP analysis was compared between the two groups using a mixed model with group and conditions as fixed factors and subjects and electrodes as random factors. The model was corrected for multiple comparisons using Bonferroni correction. Upon a significant group × condition interaction, a univariate ANOVA with group as fixed factor and subjects and electrodes as random factors were used to determine the difference in the mean total and evoked theta power between the two groups in the different conditions.

2.9 | Source reconstruction of the significant time–frequency component

A source reconstruction was performed on time course of the total and evoked theta power for the onset/offset responses of the stimulus conditions that showed a significant difference between the two

groups in the ERP analysis. This was performed the same way as previously described.

2.10 | Relationship between behavioral and neurophysiological data

The response variable for the intensity of the ZT illusion has seven distinct levels of responses going from "no ringing" to "loud and clear" which are ordered by their rank similar to a Likert-type scale (Harpe, 2015; Pell, 2005; Stevens, 1946). Thus, the rating scale of the intensity of ZT illusion may be considered as an ordinal level variable. An ordinal regression is a type of regression analysis that predicts a change between the different levels of the ordinal variable from a predictor that can be categorical, ordinal, interval, or ratio scale (Winship & Mare, 1984). In the current study, two types of analyses were performed to predict the change between the different ordinal levels of the intensity of the ZT illusion from the theta power averaged across the significant channel-time point pairs during the ZT offset response of the ERP analysis. For this, single-trial theta power (averaged between 4–7.5 Hz) was calculated. Baseline normalization was performed on each single trial and the power was converted to a decibel value using a log transformation. In the first analysis, a generalized linear model was built for an ordinal response variable with the single-trial theta power as the predictor (covariate) and the corresponding rating response of each participant from both groups in the final sample to their ZT stimulus as the dependent variable. In order to account for the variance due to a different number of trials for each person, the number of trials for each person was added as another covariate in the predictor section. Thus, the model accounts for the inter-trial and inter-subject variability. In the second analysis, the power from the single trials was averaged for each person and an ordinal regression was performed with averaged theta power as the predictor (covariate) and the median of the rating response to their ZT stimulus for each participant from both groups as a dependent variable. Such an analysis rids the data of inter-trial variability as a result of trial averaging, and tests whether there is a relationship between the neural data and the behavioral response.

3 | RESULTS

3.1 | Behavioral data

No significant differences were observed for the mean center frequency (t (14) = .97, p = .349, 95% CI = [−2,101.55739.33], Cohen's d = 0.49) and notch width (t (14) = .25, p = .805, 95% CI = [−.18 .14], Cohen's d = .13) of the ZT eliciting stimulus selected from Test A between the two groups (Figure 1). No significant difference was observed between the audiograms of the two groups either (F (15,210) = .44, p = .842, partial η^2 = .03, 95% CI for partial η^2 = [0, .06]).

3.2 | ERP analysis

No significant difference was observed in the number of ICs removed (t (14) = .58, p = .572, 95% CI = [−1.97 3.43], Cohen's d = 0.30), channels removed (t (14) = .20, p = .842, 95% CI = [−1.98 2.39], Cohen's d = 0.10), trials removed for the ZT stimulus (t (14) = 1.52, p = .150, 95% CI = [−4.67 27.46], Cohen's d = 0.71), white noise stimulus (t (14) = 1.62, p = .128, 95% CI = [−3.59 25.59], Cohen's d = 0.80) or the active control notched noise stimulus (t (14) = 1.42, p = .179, 95% CI = [−6.60 32.25], Cohen's d = 0.70) between the two groups.

We observe significant changes in the ERPs elicited in the onset and offset responses to the ZT stimulus and not to those of the white noise and notched noise stimuli (Figure 3 row 1). These statistics are shown in Table 2. In the onset response of the ZT stimulus, we observe significantly larger ERP amplitude with a negative polarity for perceivers of ZT compared to nonperceivers between 800 and 900 ms post-onset of the stimulus in a cluster of anterior electrodes as shown in the figure (Figure 3, row 3). In the offset response of the ZT stimulus, we observe significantly larger ERP amplitude with a positive polarity for perceivers of ZT compared to nonperceivers between 500 and 900 ms post-onset of the silence in a cluster of posterior electrodes as shown in the figure (Figure 3 row 3). Furthermore, we observe a significant group × condition interaction of the mean amplitude of these significant channel-time point pairs (F [1, 14] = 24.46, p < .001, partial η^2 = .70, 95% CI of partial η^2 = [.30, .76]). Independent t-tests revealed significantly larger mean amplitudes with negative and positive polarity respectively in the onset (t (14) = 3.46, p = .004, 95% CI = [.45 1.91], Cohen's d = 1.80) and offset (t (14) = −4.31, p = .001, 95% CI = [−1.84 −.62], Cohen's d = 2.22) responses of the ZT stimulus in perceivers compared to nonperceivers (Figure 3, row 2). The difference in source localized amplitude of the significant time points in the onset response (t (14) = .72, p = .07) and of offset response (t (14) = 4.38, p = .07) are marginally significant at cluster level. The figure describes the entire t-test map of both components showing changes in frontal regions such as the pgACC/vmPFC, dorsal anterior cingulate cortex (dACC), dorsolateral prefrontal cortex (DLPFC), frontal pole, temporal, and medial temporal regions such as auditory cortex and parahippocampus, parietal cortex, temporal–parietal junction, and occipital regions. A potential increase in source-level activity is observed in the dorsolateral prefrontal cortex in the onset response and in the right parietal cortex, left temporal–parietal junction, and auditory cortex in the offset response. The rest of the regions show a potential decrease in source-level activity (Figure 3, row 3).

3.3 | Time–frequency decomposition

We observed a significant group × condition interaction for the average total (F (3, 358.11) = 12.33, p < .001, partial η^2 = .09, 95% CI of partial η^2 = [.05, .14]) and evoked (F (3, 358.53) = 10.56, p < .001, partial η^2 = .08, 95% CI of partial η^2 = [.04, .12]) theta power. Further examining the group effect, we observe a significantly more positive amplitude for the mean total theta power in the ZT group in the offset response (F (1, 6.51) = 8.86, p = .022, partial η^2 = .58, 95% CI of partial
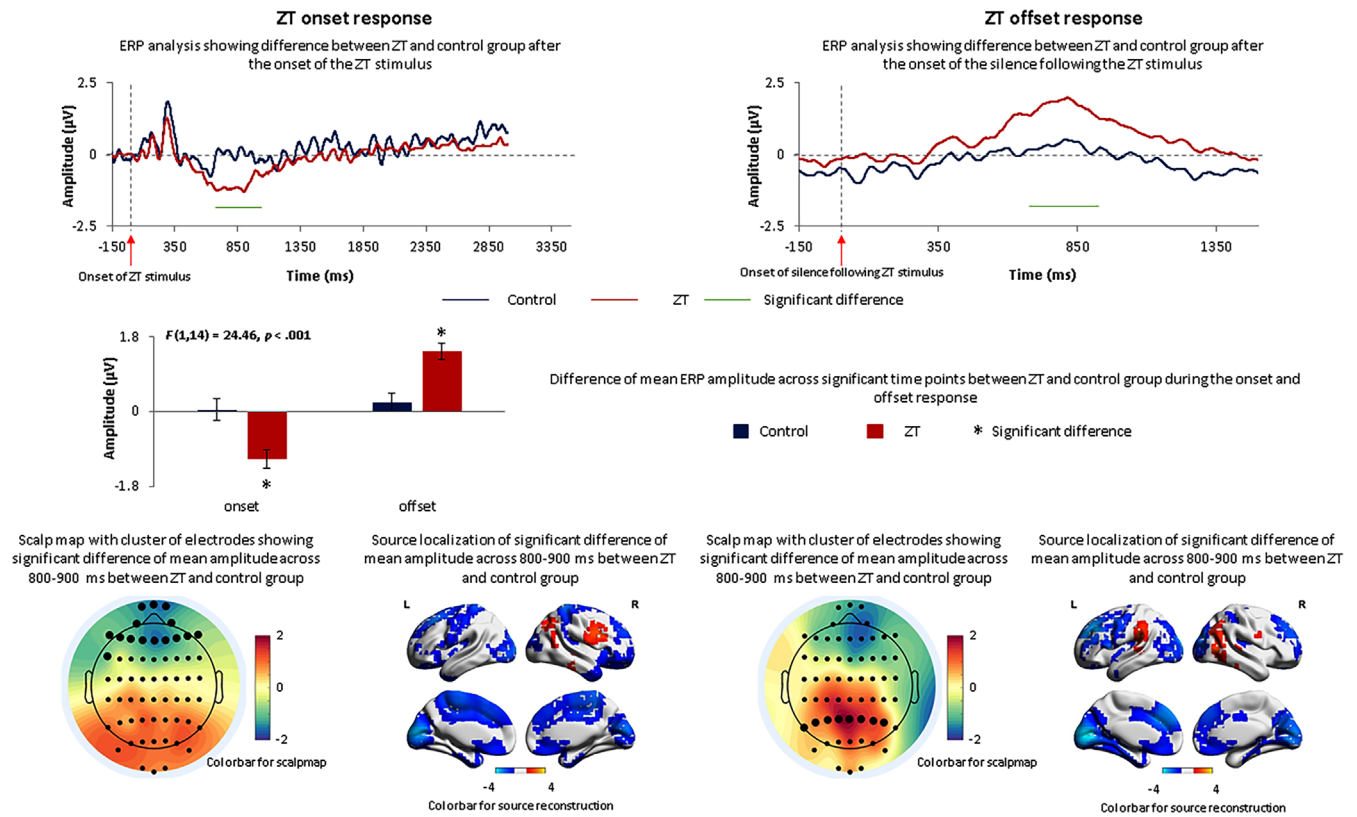
FIGURE 3 Summary of results of the grand averaged ERPs, topographic distribution and source localizations of the onset and offset responses to the ZT eliciting stimulus. Row 1 shows the grand averaged ERPs of the controls (blue line) and ZT group (red line) across the significant cluster of electrodes (shown in Row 3) and the significant difference between the two (green line). Row 2 shows the significant group × condition interaction of the mean amplitude across the significant time points shown in Row 1. The blue squares represent the control group and the red squares represent the ZT group. Row 3 shows the difference in topographical distribution and the source localization of the mean amplitude across the significant time points between the two groups. The cluster of significant electrodes is shown in BOLD. The color bar of the source localizations shows the *t*-value of the difference between the two groups

TABLE 2 Summary of cluster-based statistics comparing channel-time pairs of onset and offset ERPs between controls and ZT groups for the different stimulus conditions

Stimulus type	Onset/offset response	Positive/negative cluster	Cluster statistic	Standard deviation	*p*-value
ZT stimulus	Onset	Positive	391.73	.007	.472
ZT stimulus	Onset	Negative	−1,856.6	.002	**.022**
ZT stimulus	Offset	Positive	2,192.6	.002	**.029**
ZT stimulus	Offset	Negative	−1,034.9	.004	.107
White noise	Onset	Positive	397.69	.007	.436
White noise	Onset	Negative	−362.12	.007	.495
White noise	Offset	Positive	391.23	.007	.355
White noise	Offset	Negative	−136.63	.005	.832
Notched noise	Onset	Positive	720.82	.005	.151
Notched noise	Onset	Negative	−161.18	.004	.911
Notched noise	Offset	Positive	290.39	.007	.470
Notched noise	Offset	Negative	−103.59	.004	.915

$\eta^2 = [.06, .74]$) of the ZT stimulus and no significant difference was observed for the onset response (F (1, 6.39) = 0.12, p = .735, partial η^2 = .13, 95% CI of partial η^2 = [0, .45]). However, we observe no significant difference in the mean evoked theta power between the ZT and control groups for the ZT offset (F (1, 6.03) = 1.12, p = .33, partial η^2 = .16, 95% CI of partial η^2 = [0, .48]) and onset response (F (1, 6.07) = .002, p = .969, partial η^2 = .14, 95% CI of partial η^2 = [0, .47]). These results are shown in Figure 4, left panel.

From the scalp topographies (Figure 4, middle panel) we observe that the positivity of the mean total theta power distributes in the posterior part of the head. The source localization reveals a significant difference at the voxel level for the total theta power (t (14) = 4.39, p = .041). Figure 4, right panel, shows the entire t-test map showing changes in total theta power predominantly in the cingulate (pgACC/vmPFC, dACC, PCC), the left and right parietal cortex, frontal and temporal pole, and the parahippocampus. We observe a potential increase in total theta power in the temporal pole, left parietal cortex regions, and parahippocampus. The rest of the regions show a decrease in total theta power.

3.4 | Relationship between behavioral and neurophysiological data

The generalized linear model with an ordinal response variable as the dependent variable and single-trial theta amplitude as the predictor controlling for the number of trials for each subject is significant (Omnibus likelihood ratio χ^2 (2) = 25.10, p < .001; Test for model effects – theta power Wald χ^2 (1) = 4.03, p = .045; trials Wald χ^2 (1) = 20.45, p < .001). The ordered parameter estimates for the ordinal levels are given in Table 3. The ordered parameter estimates show the change in the response variable for one unit increase in the predictor variable (theta amplitude) controlling for the number of trials for each participant. First, we observe that one unit increase in the predictor variable significantly distinguishes the different levels in a consistent order. This satisfies the test for ordinality assumption of the response variable. Second, from the ordered parameter estimates, we observe that as the theta power increases, there is a gradual and incremental change in the behavioral response suggesting a positive relationship between single-trial theta power and ZT intensity ratings. Third, we observe that this relationship is negative in nonperceivers, positive in perceivers and the change in rating from 3 to 4 seems to form a border between perceivers and nonperceivers showing no significant change in the relationship between the behavioral response and neural activity.

From the ordinal regression between the trial-average theta amplitude and median of the behavioral response in each participant, we observe a the trend in the log-odds regression coefficients similar to the model built from the single-trial data, that is, the log-odds regression coefficients go from more negative to more positive. There also seems to be a significant relationship between the average theta power of nonperceivers with a very low rating and that of perceivers
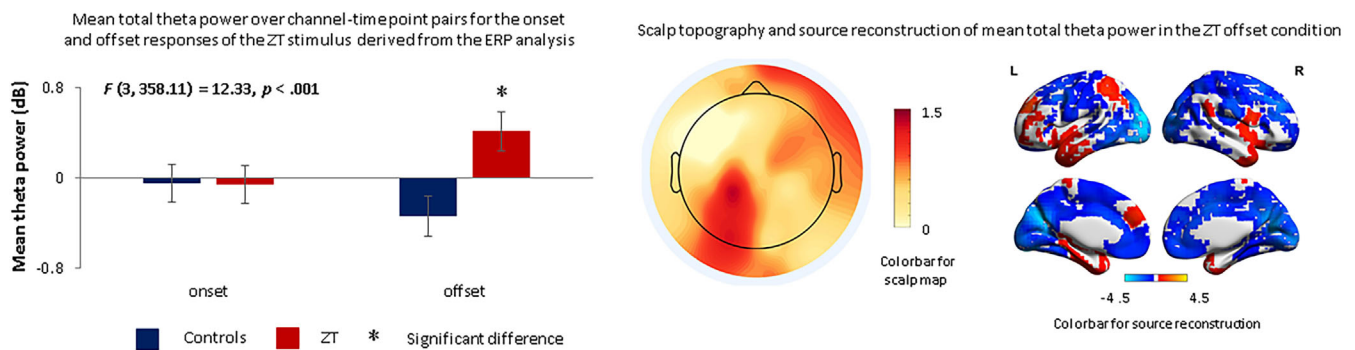

Mean total theta power over channel-time point pairs for the onset and offset responses of the ZT stimulus derived from the ERP analysis

F (3, 358.11) = 12.33, p < .001

Scalp topography and source reconstruction of mean total theta power in the ZT offset condition

FIGURE 4 Group comparison, topographic distributions and source localizations of the total theta power averaged across the significant time points and cluster of electrodes derived from the ERP analysis between the controls (blue rectangles) and ZT (red rectangles) for the onset and offset responses of the ZT stimulus. Left panel shows the significant group × condition of the mean total theta power. The blue squares represent the control group and the red squares represent the tinnitus group. Middle and right panels show the difference in topographic distributions and source localization of the mean total theta power averaged across the significant time points from the ERP analysis between the two groups. The color bar of the source localizations shows the t-value of the difference between the two groups

TABLE 3 Parameter estimates for the ordered levels of the dependent variable for the relationship between the ratings of the intensity of the ZT illusion with the single-trial theta power

Parameters	Estimate (df = 2)	Wald χ^2	p-value	CI lower	CI upper
Rating from 1 to 2	−1.29	106.75	<.001	−1.53	−1.04
Rating from 2 to 3	−0.53	21.32	<.001	−0.76	−0.31
Rating from 3 to 4	−0.04	.14	.710	−0.26	0.18
Rating from 4 to 5	0.65	32.65	<.001	0.43	0.88
Rating from 5 to 6	1.00	73.12	<.001	0.77	1.23
Rating from 6 to 7	1.58	160.81	<.001	1.34	1.83

TABLE 4 Ordinal regression log-odds regression coefficients for the relationship between the ratings of the intensity of the ZT illusion with trial-averaged theta power

Parameters	Estimate (df = 1)	Wald χ^2	p-value	CI lower	CI upper
Rating from 1 to 2	−1.60	5.06	.024	−2.99	−0.21
Rating from 2 to 3	−0.91	2.22	.136	−2.12	0.29
Rating from 3 to 4	−0.36	.38	.536	−1.48	0.77
Rating from 4 to 5	0.44	.57	.450	−0.70	1.57
Rating from 5 to 6	0.72	1.45	.228	−0.45	1.89
Rating from 6 to 7	1.39	4.08	.043	0.042	2.74

with a very high rating of ZT illusion. The ordered log-odds regression coefficients are provided in Table 4.

4 | DISCUSSION

The current study investigates the neural correlates of inducing an illusion of acute ringing in the ears (ZT illusion) following the presentation of a notched noise stimulus in a group of healthy young adults with little to no hearing loss. Among the people who perceived the illusion in the initial testing phase, some failed to reliably perceive it when the ZT stimulus was randomly interspersed with the control stimuli. This subgroup was considered the control group. There were no significant differences in the ZT illusion eliciting frequency, bandwidth or audiogram between the ZT and control groups. Furthermore, significant differences between the ERPs of the ZT and control group are observed only to the ZT eliciting stimulus and not for the control stimuli. This agrees with the behavioral data showing that when participants correctly report that they do not perceive a ringing following the control stimuli, their corresponding ERPs are not statistically different between the two groups. Thus, the difference in the neural correlates to the ZT stimulus could possibly reflect the mechanism of action of the perception of the intermittent ringing in the ZT group.

From the source localization of these differences, we observe a potential increase in source-level activity in the DLPFC following the onset of the ZT eliciting stimulus and increased activity in the auditory cortex and temporal–parietal junction following its offset in the ZT group compared to the control group. The DLPFC plays a very important role in orienting attention to a salient stimulus (Parr & Friston, 2017). The ZT eliciting stimulus has a noise notch which could be treated as a virtual deafferentation. According to the Bayesian brain theory, such a stimulus produces a prediction error (Knill & Pouget, 2004). The differential activation of the DLPFC in the ZT group, could reflect this salience and thus orientation of attention toward this stimulus. Such a theory has also been proposed in the tinnitus literature, where patients possibly attach increased salience to a prediction error (De Ridder, Vanneste, & Freeman, 2014; De Ridder, Vanneste, Weisz, et al., 2014).

Increased activity in the auditory cortex is not only shown in the perception of a ZT illusion (Leske et al., 2014) but also in the tinnitus literature (De Ridder, Congedo, & Vanneste, 2015; Ueyama et al., 2013). From a peripheral perspective this activity is suggested to reflect increased spontaneous activity in the hair cells due to loss of

sensory input (Noreña, 2011; Noreña & Farley, 2013). From a brain perspective, this activity is thought to reflect the cortical equivalent of the disinhibition of the spontaneous activity and increased prediction error (Llinás et al., 1999; Sedley et al., 2016). The phantom percept is hypothesized to be produced as a compensation to this prediction error (De Ridder, Vanneste, & Freeman, 2014). This makes sense with the increased activation of the auditory cortex during the silence period when the ZT illusion is perceived. Prediction errors are also encoded by the temporal-parietal junction. It is also involved in encoding positive symptoms such as hallucinations in patients with schizophrenia (Wible, 2012).

In addition to the DLPFC, auditory cortex and temporal-parietal junction, we also observe a potential wide-spread decrease in the activity of more frontal and cingulate regions such as the dACC, pgACC/vmPFC, and medial temporal regions such as the parahippocampus. The dACC works together with the DLPFC in orienting attention toward a salient stimulus (Seeley et al., 2007). The pgACC/vmPFC and the parahippocampus form an integral part of the sensory gating system that inhibits unwanted stimuli which is shown to be altered in tinnitus patients using task-based and resting-state EEG studies (Campbell et al., 2018; Hong et al., 2012; Vanneste, Alsalman, & De Ridder, 2018; Vanneste, Alsaman, & De Ridder, 2018). In addition, we also observe changes in activity in the occipital and somatosensory regions during the presentation of the stimulus and perception of the illusion. Interaction of cross-modal sensory system in tinnitus is currently under study (Ralli et al., 2017; Shore & Wu, 2019) and this may be relevant to the perception of a ZT illusion. This, however, cannot be answered using the current paradigm.

The time–frequency analysis focuses on the theta frequency band for several reasons. Increased theta activity in the auditory cortex is proposed to be a marker of decreased inhibition due to increased spontaneous activity following sensory deafferentation (De Ridder, Vanneste, et al., 2015). The theta activity acts as a carrier wave for gamma activity which is correlated with the intensity of phantom percept (Vanneste, Alsaman, & De Ridder, 2018; Vanneste & De Ridder, 2016). Furthermore, theta activity in the parahippocampus is correlated with the amount of hearing loss in tinnitus patients (Vanneste & De Ridder, 2016). Increased theta activity in the pgACC/vmPFC, parahippocampus, and hippocampus is also a marker for decreased gating of unwanted stimuli in patients with tinnitus and schizophrenia (Brockhaus-Dumke, Mueller, Faigle, & Klosterkoetter, 2008; Hong et al., 2012; Vanneste, Alsalman, & De Ridder, 2018; Vanneste, Alsaman, & De Ridder, 2018).

In the current study, we observe that the total theta power in the offset response of the ZT stimulus is significantly greater in the ZT group compared to the control group. We, however, do not observe the same for evoked power. The total theta power is calculated from single trials and thus reflects a combination of both time-locked and non timelocked theta activity whereas the evoked power strictly represents the time-locked activity. This could mean that the ZT perception induces/influences ongoing theta oscillations rather than evoke them in a phase-locked manner. The total theta power localized on to the source space shows potentially increased theta activity in the temporal and frontal pole, orbitofrontal cortex, temporal-parietal junction, parts of the pgACC/vmPFC region, and the parahippocampus. The increased theta activity in the parahippocampus, pgACC/vmPFC, orbital frontal cortex regions that form a part of the "noise-cancelation" sensory gating system could suggest a breakdown of this system during the perception of the hallucination (Rauschecker et al., 2015; Rauschecker, Leaver, & Mühlau, 2010; Vanneste, Alsalman, & De Ridder, 2018, 2019). This also supports the idea that more top-down systems may be involved during the perception of an acute phantom ringing especially in participants with no audiometric hearing loss. The frontal and temporal poles have been widely reported in tinnitus literature. The frontal pole is reported with the orbitofrontal cortex in the frontostriatal gating system and the temporal pole as a part of the auditory network encoding the phantom percept (Chen et al., 2015; Leaver et al., 2012; Sedley et al., 2015).

In addition to sensory gating, the parahippocampus is also proposed to hold the auditory memory (De Ridder et al., 2006; Munoz-Lopez et al., 2010). According to the Bayesian brain theory, the parahippocampus is involved in pulling sounds out of the auditory memory to compensate for the missing sensory information (De Ridder et al., 2011; De Ridder, Vanneste, & Freeman, 2014). This could supposedly be what's happening with inducing the ZT illusion since the ringing is shown to mirror the missing frequencies (Noreña & Eggermont, 2003). The most compelling finding of the current study is the significant positive relationship between ZT intensity rating and single-trial theta power showing that ZT illusions may be related to changes in higher-order processing systems such as sensory gating and auditory memory recall. A link between changing low-frequency oscillations and perception of auditory illusions has been shown in a recent study by Kaiser and colleagues (Kaiser, Senkowski, Roa Romero, Riecke, & Keil, 2018). In this article, they show that reduced theta power goes together with the perceptual restoration of a tone when a temporal gap is masked by adding noise. This may be thought as complementary to the findings of the current study, where increased theta power is associated with a continual perception of a tone following a spectral gap (i.e., removing noise). The gradual change from a negative relationship to a positive relationship distinguishing the different levels of response illustrates that perceivers and non-perceivers present a diametrically opposite trend. The no relationship between theta power and change in rating between 3 and 4 is interesting because it creates a data-driven divide between perceivers and non-perceivers. Further research on this divide may be interesting to see if there may be an objective and tangible measure that could be extracted to predict if someone may be able to reliably perceive a ZT illusion. This may be an important translation to tinnitus when understanding the transition from acute to chronic tinnitus.

The findings of the current study may also reflect the neural correlates of conscious and nonconscious processing of stimuli further suggesting the involvement of changes in higher-order processing of ZT illusions. Salti and colleagues suggest that conscious perception of stimuli is distinguished by an amplification of incoming sensory information, possibly through reverberating loops (Lamme, 2006; Salti et al., 2015), and its distributed representation in multiple distinct regions including parietal and prefrontal cortices, which are part of the so-called global workspace (Dehaene, Changeux, Naccache, Sackur, & Sergent, 2006; Dehaene & Naccache, 2001). The "global workspace" is a cognitive architecture introduced by Baars to account for conscious and unconscious processing (Baars, 2005; Baars, Ramsøy, & Laureys, 2003; Shanahan & Baars, 2005). Other researchers proposed a set of regions that may be involved in bringing stimuli into conscious perception (Dehaene & Changeux, 2011; Dehaene, Kerszberg, & Changeux, 1998; Dehaene & Naccache, 2001; Salti et al., 2015). Such a conscious perception is encoded by increased theta activity (Doesburg, Green, McDonald, & Ward, 2009; Melloni et al., 2007; Nakatani, Raffone, & van Leeuwen, 2014; Sitt et al., 2014), which is also the frequency range of slow positive event-related potentials, such as the P3. Conversely, unconscious information fails to be sequentially dispatched to the successive steps of a serial task and, therefore, remains blocked within a fixed representational state, where it slowly decays (Salti et al., 2015). This is consistent with the results of the current study. Here, we observe changes (increase and decrease) in total theta activity in widespread frontoparietal regions which are all part of the global workspace in the time frame of the late potential (Baars, 2005; Dehaene et al., 1998; Dehaene & Naccache, 2001). Thus, the difference between the two groups during ZT perception may reflect the changes in the amplification of sensory information, or in Bayesian terms increased salience of prediction error, and the differential activation of the global workspace. This may be an explanation as to why the control group does not perceive the ZT illusion when stimuli are presented in random order.

Compared to previous studies which present their stimulus at 40–50 dB SPL, we present our stimulus at a higher intensity. Although it is possible to argue that this may be the reason we do not see 100% ZT illusion perception, another group has also shown that there are people who reliably perceive the ZT illusion and people who do not even at 50 dB SPL (DeGuzman, 2012). Hence, the neural changes presented here may truly reflect a difference in higher-order processing between the two groups of participants. In this regard, the origin and mechanism of the ZT illusion are important to understanding the mechanism of tinnitus. Previous studies have reported that ZT illusions are accompanied by changes in lateral inhibition and nonlinear gain around the frequencies surrounding the notch (Parra & Pearlmutter, 2007; Zeng, 2013). If this were alone the reason, then everyone would have been able to perceive an illusion. It is important to keep in mind that the participants do not have audiometric hearing loss. Thus, the ZT illusion may be a more top-down process of decreased sensory

gating and filling for the missing information. However, this is not to say that other bottom-up changes may not be present in the ZT group. There is abundant literature around "hidden" hearing loss and changes in the auditory pathways that are not detected by an audiogram (Schaette & McAlpine, 2011). Thus, future studies also taking into consideration auditory brainstem responses to detect "hidden" hearing loss could better clarify this point. In addition, inspecting ZT illusions in tinnitus patients with no hearing loss compared to perceivers and non-perceivers without tinnitus could also provide more insight into the relationship between ZT illusion and tinnitus, helping understand the mechanism of action of auditory phantoms. Furthermore, longitudinal studies on a larger sample, following up participants with a ZT illusion to see if they go on to develop tinnitus could be confirmation to whether ZT illusions may be a precursor to developing chronic tinnitus. Such a study would be crucial in identifying the population who are at a higher risk of developing chronic tinnitus. This is important for the development of preventative care.

5 | CONCLUSION

The current study investigates the effects of inducing intermittent ZT illusion on the functionality of brain regions. We observed changes in activity in wide-spread regions in the brain particularly the cingulate, auditory and medial temporal regions like the parahippocampus during the perception of the ZT illusion. These regions are of particular interest as they suggest a disinhibition of the sensory cortices together with a dysregulated sensory gating system in participants who reliably perceive the ZT illusion. This hypothesis is further supported by an increase in theta activity in the same regions during the perception of the illusion. Increased theta activity in the parahippocampus suggests a successful retrieval of the memory of the missing frequencies of the notch and bringing it to conscious perception. Furthermore, increased theta activity significantly predicts a positive change in the intensity of the ZT rating which further supports the hypothesis of a potential breakdown of higher-order processing systems.

CONFLICT OF INTEREST
The authors declare no conflict of interest.

DATA AVAILABILITY STATEMENT
The data is available with the corresponding author and will be available on request.

ORCID
Anusha Mohan https://orcid.org/0000-0003-1904-0603

REFERENCES
Baars, B. J. (2005). Global workspace theory of consciousness: Toward a cognitive neuroscience of human experience. *Progress in Brain Research*, *150*, 45–53.

Baars, B. J., Ramsøy, T. Z., & Laureys, S. (2003). Brain, conscious experience and the observing self. *Trends in Neurosciences*, *26*, 671–675.

Brett, M., Johnsrude, I. S., & Owen, A. M. (2002). The problem of functional localization in the human brain. *Nature Reviews Neuroscience*, *3*, 243–249.

Brockhaus-Dumke, A., Mueller, R., Faigle, U., & Klosterkoetter, J. (2008). Sensory gating revisited: Relation between brain oscillations and auditory evoked potentials in schizophrenia. *Schizophrenia Research*, *99*, 238–249.

Campbell, J., Bean, C., & LaBrec, A. (2018). Normal hearing young adults with mild tinnitus: Reduced inhibition as measured through sensory gating. *Audiology Research*, *8*, 214–214.

Catz, N., & Noreña, A. J. (2013). Enhanced representation of spectral contrasts in the primary auditory cortex. *Frontiers in Systems Neuroscience*, *7*, 21–21.

Cederroth, C. R., Gallus, S., Hall, D. A., Kleinjung, T., Langguth, B., Maruotti, A., ... Schlee, W. (2019). Editorial: Towards an understanding of tinnitus heterogeneity. *Frontiers in Aging Neuroscience*, *11*, 53.

Chen, Y.-C., Xia, W., Feng, Y., Li, X., Zhang, J., Feng, X., ... Salvi, R. (2015). Altered interhemispheric functional coordination in chronic tinnitus patients. *BioMed Research International*, *2015*, 345647.

Claes, L., Stamberger, H., Van de Heyning, P., De Ridder, D., & Vanneste, S. (2014). Auditory cortex tACS and tRNS for tinnitus: Single versus multiple sessions. *Neural Plasticity*, *2014*, 436713.

Cohen, M. X. (2014). *Analyzing neural time series data: Theory and practice*. Cambridge, MA: MIT Press.

De Ridder, D., Congedo, M., & Vanneste, S. (2015). The neural correlates of subjectively perceived and passively matched loudness perception in auditory phantom perception. *Brain and Behavior: A Cognitive Neuroscience Perspective*, *5*, e00331.

De Ridder, D., Elgoyhen, A. B., Romo, R., & Langguth, B. (2011). Phantom percepts: Tinnitus and pain as persisting aversive memory networks. *Proceedings of the National Academy of Sciences*, *108*, 8075–8080.

De Ridder, D., Fransen, H., Francois, O., Sunaert, S., Kovacs, S., & Van De Heyning, P. (2006). Amygdalohippocampal involvement in tinnitus and auditory memory. *Acta Oto-Laryngologica*, *126*, 50–53.

De Ridder, D., & Vanneste, S. (2014). Targeting the Parahippocampal area by auditory cortex stimulation in tinnitus. *Brain Stimulation*, *7*, 709–717.

De Ridder, D., Vanneste, S., & Freeman, W. (2014). The Bayesian brain: Phantom percepts resolve sensory uncertainty. *Neuroscience & Biobehavioral Reviews*, *44*, 4–15.

De Ridder, D., Vanneste, S., Langguth, B., & Llinas, R. (2015). Thalamocortical dysrhythmia: A theoretical update in tinnitus. *Frontiers in Neurology*, *6*, 124.

De Ridder, D., Vanneste, S., Weisz, N., Londero, A., Schlee, W., Elgoyhen, A. B., & Langguth, B. (2014). An integrative model of auditory phantom perception: Tinnitus as a unified percept of interacting separable subnetworks. *Neuroscience and Biobehavioral Reviews*, *44*, 16–32.

DeGuzman, P. J. S. (2012). *Neural correlates of phantom auditory perception*. New York NY: CUNY Academic Works.

Dehaene, S., & Changeux, J.-P. (2011). Experimental and theoretical approaches to conscious processing. *Neuron*, *70*, 200–227.

Dehaene, S., Changeux, J.-P., Naccache, L., Sackur, J., & Sergent, C. (2006). Conscious, preconscious, and subliminal processing: A testable taxonomy. *Trends in Cognitive Sciences*, *10*, 204–211.

Dehaene, S., Kerszberg, M., & Changeux, J.-P. (1998). A neuronal model of a global workspace in effortful cognitive tasks. *Proceedings of the National Academy of Sciences*, *95*, 14529–14534.

Dehaene, S., & Naccache, L. (2001). Towards a cognitive neuroscience of consciousness: Basic evidence and a workspace framework. *Cognition*, *79*, 1–37.

Dehmel, S., Eisinger, D., & Shore, S. (2012). Gap prepulse inhibition and auditory brainstem-evoked potentials as objective measures for tinnitus in Guinea pigs. *Frontiers in Systems Neuroscience*, *6*, 42.

Doesburg, S. M., Green, J. J., McDonald, J. J., & Ward, L. M. (2009). Rhythms of consciousness: Binocular rivalry reveals large-scale oscillatory network dynamics mediating visual perception. *PLoS One*, *4*, e6142.

Freedman, R., Adler, L. E., Myles-Worsley, M., Nagamoto, H. T., Miller, C., Kisley, M., ... Waldo, M. (1996). Inhibitory gating of an evoked response to repeated auditory stimuli in schizophrenic and Normal subjects: Human recordings, computer simulation, and an animal model. *JAMA Psychiatry*, *53*, 1114–1121.

Friston, K. (2005). A theory of cortical responses. *Philosophical Transactions of the Royal Society, B: Biological Sciences*, *360*, 815–836.

Friston, K. (2010). The free-energy principle: A unified brain theory? *Nature Reviews Neuroscience*, *11*, 127–138.

Friston, K., FitzGerald, T., Rigoli, F., Schwartenbeck, P., O'Doherty, J., & Pezzulo, G. (2016). Active inference and learning. *Neuroscience & Biobehavioral Reviews*, *68*, 862–879.

Friston, K., Kilner, J., & Harrison, L. (2006). A free energy principle for the brain. *Journal of Physiology, Paris*, *100*, 70–87.

Fuchs, M., Kastner, J., Wagner, M., Hawes, S., & Ebersole, J. S. (2002). A standardized boundary element method volume conductor model. *Clinical Neurophysiology*, *113*, 702–712.

Harpe, S. E. (2015). How to analyze Likert and other rating scale data. *Currents in Pharmacy Teaching & Learning*, *7*, 836–850.

Hong, L. E., Summerfelt, A., Mitchell, B. D., O'Donnell, P., & Thaker, G. K. (2012). A shared low-frequency oscillatory rhythm abnormality in resting and sensory gating in schizophrenia. *Clinical Neurophysiology*, *123*, 285–292.

Hullfish, J., Abenes, I., Kovacs, S., Sunaert, S., De Ridder, D., & Vanneste, S. (2018a). Functional brain changes in auditory phantom perception evoked by different stimulus frequencies. *Neuroscience Letters*, *683*, 160–167.

Hullfish, J., Abenes, I., Kovacs, S., Sunaert, S., De Ridder, D., & Vanneste, S. (2018b). Functional connectivity analysis of fMRI data collected from human subjects with chronic tinnitus and varying levels of tinnitus-related distress. *Data in Brief*, *21*, 779–789.

Hullfish, J., Abenes, I., Yoo, H. B., De Ridder, D., & Vanneste, S. (2019). Frontostriatal network dysfunction as a domain-general mechanism underlying phantom perception. *Human Brain Mapping*, *40*, 2241–2251.

Hullfish, J., Sedley, W., & Vanneste, S. (2019). Prediction and perception: Insights for (and from) tinnitus. *Neuroscience & Biobehavioral Reviews*, *102*, 1–12.

Husain, F. T., Medina, R. E., Davis, C. W., Szymko-Bennett, Y., Simonyan, K., Pajor, N. M., & Horwitz, B. (2011). Neuroanatomical changes due to hearing loss and chronic tinnitus: A combined VBM and DTI study. *Brain Research*, *1369*, 74–88.

Jastreboff, P. J. (1990). Phantom auditory perception (tinnitus): Mechanisms of generation and perception. *Neuroscience Research*, *8*, 221–254.

Jastreboff, P. J., Sasaki, C. T., & Brennan, J. F. (1988). An animal model for tinnitus. *The Laryngoscope*, *98*, 280–286.

Jung, T.-P., Makeig, S., Bell, A. J., & Sejnowski, T. J. (1998). Independent component analysis of electroencephalographic and event-related potential data. In P. W. F. Poon & J. F. Brugge (Eds.), *Central auditory processing and neural modeling* (pp. 189–197). Boston, MA: Springer.

Jurcak, V., Tsuzuki, D., & Dan, I. (2007). 10/20, 10/10, and 10/5 systems revisited: Their validity as relative head-surface-based positioning systems. *NeuroImage*, *34*, 1600–1611.

Kaiser, M., Senkowski, D., Roa Romero, Y., Riecke, L., & Keil, J. (2018). Reduced low-frequency power and phase locking reflect restoration in the auditory continuity illusion. *European Journal of Neuroscience*, *48*, 2849–2856.

Knill, D. C., & Pouget, A. (2004). The Bayesian brain: The role of uncertainty in neural coding and computation. *Trends in Neurosciences*, *27*, 712–719.

König, O., Schaette, R., Kempter, R., & Gross, M. (2006). Course of hearing loss and occurrence of tinnitus. *Hearing Research*, *221*, 59–64.

Krause, M., Hoffmann, W. E., & Hajós, M. (2003). Auditory sensory gating in hippocampus and reticular thalamic neurons in anesthetized rats. *Biological Psychiatry*, *53*, 244–253.

Lamme, V. A. F. (2006). Towards a true neural stance on consciousness. *Trends in Cognitive Sciences*, *10*, 494–501.

Lancaster, J. L., Woldorff, M. G., Parsons, L. M., Liotti, M., Freitas, C. S., Rainey, L., ... Fox, P. T. (2000). Automated Talairach atlas labels for functional brain mapping. *Human Brain Mapping*, *10*, 120–131.

Leaver, A., Seydell-Greenwald, A., Turesky, T., Morgan, S., Kim, H., & Rauschecker, J. (2012). Cortico-limbic morphology separates tinnitus from tinnitus distress. *Frontiers in Systems Neuroscience*, *6*, 21.

Leske, S., Tse, A., Oosterhof, N. N., Hartmann, T., Müller, N., Keil, J., & Weisz, N. (2014). The strength of alpha and beta oscillations parametrically scale with the strength of an illusory auditory percept. *NeuroImage*, *88*, 69–78.

Llinás, R., Urbano, F. J., Leznik, E., Ramírez, R. R., & van Marle, H. J. (2005). Rhythmic and dysrhythmic thalamocortical dynamics: GABA systems and the edge effect. *Trends in Neurosciences*, *28*, 325–333.

Llinás, R. R., Ribary, U., Jeanmonod, D., Kronberg, E., & Mitra, P. P. (1999). Thalamocortical dysrhythmia: A neurological and neuropsychiatric syndrome characterized by magnetoencephalography. *Proceedings of the National Academy of Sciences*, *96*, 15222–15227.

Mazziotta, J., Toga, A., Evans, A., Fox, P., Lancaster, J., Zilles, K., ... Mazoyer, B. (2001). A probabilistic atlas and reference system for the human brain: International consortium for brain mapping (ICBM). *Philosophical Transactions of the Royal Society of London, Series B*, *356*, 1293–1322.

Melloni, L., Molina, C., Pena, M., Torres, D., Singer, W., & Rodriguez, E. (2007). Synchronization of neural activity across cortical areas correlates with conscious perception. *The Journal of Neuroscience*, *27*, 2858–2865.

Mohan, A., Alexandra, S. J., Johnson, C. V., De Ridder, D., & Vanneste, S. (2018). Effect of distress on transient network dynamics and topological equilibrium in phantom sound perception. *Progress in Neuro-Psychopharmacology & Biological Psychiatry*, *84*, 79–92.

Mohan, A., De Ridder, D., Idiculla, R., DSouza, C., & Vanneste, S. (2018). Distress-dependent temporal variability of regions encoding domain-specific and domain-general behavioral manifestations of phantom percepts. *The European Journal of Neuroscience*, *48*, 1743–1764.

Mohan, A., De Ridder, D., & Vanneste, S. (2016). Graph theoretical analysis of brain connectivity in phantom sound perception. *Scientific Reports*, *6*, 19683.

Mohan, A., De Ridder, D., & Vanneste, S. (2017). Robustness and dynamicity of functional networks in phantom sound. *NeuroImage*, *146*, 171–187.

Mohan, A., & Vanneste, S. (2017). Adaptive and maladaptive neural compensatory consequences of sensory deprivation—From a phantom percept perspective. *Progress in Neurobiology*, *153*, 1–17.

Munoz-Lopez, M. M., Mohedano-Moriano, A., & Insausti, R. (2010). Anatomical pathways for auditory memory in primates. *Frontiers in Neuroanatomy*, *4*, 129.

Nakatani, C., Raffone, A., & van Leeuwen, C. (2014). Efficiency of conscious access improves with coupling of slow and fast neural oscillations. *Journal of Cognitive Neuroscience*, *26*, 1168–1179.

Negri, B., & Schorn, K. (1991). Noise-induced hearing loss and tinnitus. *HNO*, *39*, 192–194.

Norena, A., & Eggermont, J. (2003). Neural correlates of an auditory afterimage in primary auditory cortex. *Journal of the Association for Research in Otolaryngology*, *4*, 312–328.

Norena, A., Micheyl, C., & Chery-Croze, S. (2000). An auditory negative after-image as a human model of tinnitus. *Hearing Research*, *149*, 24–32.

Noreña, A. J. (2011). An integrative model of tinnitus based on a central gain controlling neural sensitivity. *Neuroscience & Biobehavioral Reviews*, *35*, 1089–1109.

Noreña, A. J., & Eggermont, J. J. (2003). Neural correlates of an auditory afterimage in primary auditory cortex. *Journal of the Association for Research in Otolaryngology*, *4*, 312–328.

Noreña, A. J., & Farley, B. J. (2013). Tinnitus-related neural activity: Theories of generation, propagation, and centralization. *Hearing Research*, *295*, 161–171.

Oostenveld, R., & Maris, E. (2007). Nonparametric statistical testing of EEG-and MEG-data. *Journal of Neuroscience Methods*, *164*(1), 177–190.

Parr, T., & Friston, K. J. (2017). Working memory, attention, and salience in active inference. *Scientific Reports*, *7*, 14678.

Parra, L. C., & Pearlmutter, B. A. (2007). Illusory percepts from auditory adaptation. *The Journal of the Acoustical Society of America*, *121*, 1632–1641.

Pascual-Marqui, R. D. (2002). Standardized low-resolution brain electromagnetic tomography (sLORETA): Technical details. *Methods and Findings in Experimental and Clinical Pharmacology*, *24*, 5–12.

Peelle, J. E., & Wingfield, A. (2016). The neural consequences of age-related hearing loss. *Trends in Neurosciences*, *39*, 486–497.

Pell, G. (2005). Use and misuse of Likert scales. *Medical Education*, *39*, 970–970.

Ralli, M., Greco, A., Turchetta, R., Altissimi, G., de Vincentiis, M., & Cianfrone, G. (2017). Somatosensory tinnitus: Current evidence and future perspectives. *The Journal of International Medical Research*, *45*, 933–947.

Rauschecker, J. P., Leaver, A. M., & Muhlau, M. (2010). Tuning out the noise: Limbic-auditory interactions in tinnitus. *Neuron*, *66*, 819–826.

Rauschecker, J. P., Leaver, A. M., & Mühlau, M. (2010). Tuning out the noise: Limbic-auditory interactions in tinnitus. *Neuron*, *66*, 819–826.

Rauschecker, J. P., May, E. S., Maudoux, A., & Ploner, M. (2015). Fronto-striatal gating of tinnitus and chronic pain. *Trends in Cognitive Sciences*, *19*, 567–578.

Salti, M., Monto, S., Charles, L., King, J.-R., Parkkonen, L., & Dehaene, S. (2015). Distinct cortical codes and temporal dynamics for conscious and unconscious percepts. *eLife*, *4*, e05652.

Schacter, D. L. (2011). *Psychology* (2nd ed.). New York, NY: Worth Publishers.

Schaette, R., & McAlpine, D. (2011). Tinnitus with a normal audiogram: Physiological evidence for hidden hearing loss and computational model. *Journal of Neuroscience*, *31*, 13452–13457.

Sedley, W., Friston, K. J., Gander, P. E., Kumar, S., & Griffiths, T. D. (2016). An integrative tinnitus model based on sensory precision. *Trends in Neurosciences*, *39*, 799–812.

Sedley, W., Gander, P. E., Kumar, S., Kovach, C. K., Oya, H., Kawasaki, H., … Griffiths, T. D. (2016). Neural signatures of perceptual inference. *eLife*, *5*, e11476.

Sedley, W., Gander, P. E., Kumar, S., Oya, H., Kovach, C. K., Nourski, K. V., … Griffiths, T. D. (2015). Intracranial mapping of a cortical tinnitus system using residual inhibition. *Current Biology*, *25*, 1208–1214.

Sedley, W., Parikh, J., Edden, R. A., Tait, V., Blamire, A., & Griffiths, T. D. (2015). Human auditory cortex neurochemistry reflects the presence and severity of tinnitus. *The Journal of Neuroscience, 35*, 14822–14828.

Seeley, W. W., Menon, V., Schatzberg, A. F., Keller, J., Glover, G. H., Kenna, H., … Greicius, M. D. (2007). Dissociable intrinsic connectivity networks for salience processing and executive control. *The Journal of Neuroscience*, *27*, 2349–2356.

Shanahan, M., & Baars, B. (2005). Applying global workspace theory to the frame problem. *Cognition*, *98*, 157–176.

Shore, S. E., Roberts, L. E., & Langguth, B. (2016). Maladaptive plasticity in tinnitus-triggers, mechanisms and treatment. *Nature Reviews. Neurology*, *12*, 150–160.

Shore, S. E., & Wu, C. (2019). Mechanisms of noise-induced tinnitus: Insights from cellular studies. *Neuron*, *103*, 8–20.

Sitt, J. D., King, J.-R., El Karoui, I., Rohaut, B., Faugeras, F., Gramfort, A., … Naccache, L. (2014). Large scale screening of neural signatures of consciousness in patients in a vegetative or minimally conscious state. *Brain*, *137*, 2258–2270.

Stevens, S. S. (1946). On the theory of scales of measurement. *Science*, *103*, 677–680.

Talairach, J., Tournoux, P. (1988). *Co-planar Stereotaxic Atlas of the Human Brain*. Georg Thieme Verlag, Stuttgart.

Turner, J. G., Brozoski, T. J., Bauer, C. A., Parrish, J. L., Myers, K., Hughes, L. F., & Caspary, D. M. (2006). Gap detection deficits in rats with tinnitus: A potential novel screening tool. *Behavioral Neuroscience*, *120*, 188–195.

Ueyama, T., Donishi, T., Ukai, S., Ikeda, Y., Hotomi, M., Yamanaka, N., … Kaneoke, Y. (2013). Brain regions responsible for tinnitus distress and loudness: A resting-state fMRI study. *PLoS One*, *8*, e67778.

Vanneste, S., Alsalman, O., & De Ridder, D. (2018). COMT and the neurogenetic architecture of hearing loss induced tinnitus. *Hearing Research*, *365*, 1–15.

Vanneste, S., Alsalman, O., & De Ridder, D. (2019). Top-down and bottom-up regulated auditory phantom perception. *The Journal of Neuroscience*, *39*, 364–378.

Vanneste, S., Alsaman, O., & De Ridder, D. (2018). Top-down and bottom-up regulated auditory phantom perception. *The Journal of Neuroscience*, *39*, 364–378.

Vanneste, S., & De Ridder, D. (2016). Deafferentation-based pathophysiological differences in phantom sound: Tinnitus with and without hearing loss. *NeuroImage*, *129*, 80–94.

Vilares, I., & Kording, K. (2011). Bayesian models: The structure of the world, uncertainty, behavior, and the brain. *Annals of the New York Academy of Sciences*, *1224*, 22–39.

Wang, H., Brozoski, T. J., & Caspary, D. M. (2011). Inhibitory neurotransmission in animal models of tinnitus: Maladaptive plasticity. *Hearing Research*, *279*, 111–117.

Wible, C. G. (2012). Hippocampal temporal-parietal junction interaction in the production of psychotic symptoms: A framework for understanding the schizophrenic syndrome. *Frontiers in Human Neuroscience*, *6*, 180.

Winkler, I., Denham, S., & Escera, C. (2013). Auditory event-related potentials. In D. Jaeger & R. Jung (Eds.), *Encyclopedia of computational neuroscience* (pp. 1–29). New York, NY: Springer.

Winship, C., & Mare, R. D. (1984). Regression models with ordinal variables. *American Sociological Review*, *49*, 512–525.

Zeng, F.-G. (2013). An active loudness model suggesting tinnitus as increased central noise and hyperacusis as increased nonlinear gain. *Hearing Research*, *295*, 172–179.

Zwicker, E. (1964). "Negative afterimage" in hearing. *The Journal of the Acoustical Society of America*, *36*, 2413–2415.